Nanoscale c3nr03982j

## PAPER

50

Gadolinium oxysulfide nanoparticles as multimodal imaging agents for $T_2$ -weighted MR, X-ray tomography and photoluminescence
Sèmiyou. A. Osseni, Sévérine Lechevallier, Marc Verelst, Pascal Perriat, Jeannette Dexpert-Ghys, David Neumeyer, Robin Garcia, Florian Mayer, Kristina Djanashvili, Joop A. Peters, Eddy Magdeleine, Hélène Gros-Dagnac, Pierre Celsis and Robert Mauricot*
Doped $Gd_2O_2S$ NPs were proposed as new multimodal imaging agents for $T_2$ -weighted MR, X-ray tomography and photoluminescence imaging.
Please check this proof carefully. Our staff will not read it in detail after you have returned it.
Translation errors between word-processor files and typesetting systems can occur so the whole proof needs to be read. Please pay particular attention to: tabulated material; equations; numerical data; figures and graphics; and references. If you have not already indicated the corresponding author(s) please mark their name(s) with an asterisk. Please e-mail a list of corrections or the PDF with electronic notes attached – do not change the text within the PDF file or send a revised manuscript. Corrections at this stage should be minor and not involve extensive changes. All corrections must be sent at the same time.
Please bear in mind that minor layout improvements, e.g. in line breaking, table widths and graphic placement, are routinely applied to the final version.
We will publish articles on the web as soon as possible after receiving your corrections; no late corrections will be made.
Please return your final corrections, where possible within 48 hours of receipt by e-mail to: nanoscale@rsc.org

# **Queries for the attention of the authors**

Journal: Nanoscale

<sup>5</sup> Paper: **c3nr03982j** 

Title: Gadolinium oxysulfide nanoparticles as multimodal imaging agents for  $T_2$ -weighted MR, X-ray tomography and photoluminescence

1

5

10

Editor's queries are marked like this... , and for your convenience line numbers are inserted like this... 5

Please ensure that all queries are answered when returning your proof corrections so that publication of your article is not delayed.

15	Query Reference	Query	Remarks	15
20	1	For your information: You can cite this article before you receive notification of the page numbers by using the following format: (authors), Nanoscale, (year), DOI: 10.1039/c3nr03982j.		20
25	2	Please carefully check the spelling of all author names. This is important for the correct indexing and future citation of your article. No late corrections can be made.		25
	3	Please check that the GA text fits within the allocated space indicated on the front page of the proof. If the entry does not fit between the two horizontal lines, then please trim the text and/or the title.		20
30	4	The meaning of the phrase "sensibly better" in the sentence beginning "Our study shows that…" is not clear – please clarify.		30
35	5	In the sentence beginning "However, the ionic strength" should "avoiding" be changed to "preventing"?		35
	6	Ref. 12: Please provide the initial(s) for the 9th author.		

40

45

50

Nanoscale RSCPublishing

# **PAPER**

1	
	fi

Cite this: DOI: 10.1039/c3nr03982j

### 10

15

20

25

30

35

40

45

Received 31st July 2013 Accepted 18th October 2013

DOI: 10.1039/c3nr03982j

www.rsc.org/nanoscale

# Gadolinium oxysulfide nanoparticles as multimodal imaging agents for $T_2$ -weighted MR, X-ray tomography and photoluminescence †

Sèmiyou. A. Osseni,<sup>a</sup> Sévérine Lechevallier,<sup>a</sup> Marc Verelst,<sup>a</sup> Pascal Perriat,<sup>b</sup> Jeannette Dexpert-Ghys,<sup>a</sup> David Neumeyer,<sup>a</sup> Robin Garcia,<sup>c</sup> Florian Mayer,<sup>d</sup> Kristina Djanashvili,<sup>d</sup> Joop A. Peters,<sup>d</sup> Eddy Magdeleine,<sup>e</sup> Hélène Gros-Dagnac,<sup>f</sup> Pierre Celsis<sup>f</sup> and Robert Mauricot\*<sup>a</sup>

We have synthesized gadolinium oxysulfide nanoparticles (NPs) doped with other lanthanides (Eu<sup>3+</sup>, Er<sup>3+</sup>, Yb<sup>3+</sup>) via a hydroxycarbonate precursor precipitation route followed by a sulfuration process under a H<sub>2</sub>S–Ar atmosphere at 750 °C in order to propose new multimodal nanoplatforms for Magnetic Resonance (MR), X-ray and photoluminescence imaging. Gd<sub>2</sub>O<sub>2</sub>S:Eu<sup>3+</sup> NPs strongly absorb near UV ( $\approx$ 300–400 nm) and re-emit strong red light (624 nm). They can be easily internalized by cancer cells, and imaged by epifluorescence microscopy under excitation in the NUV (365 nm). They are not cytotoxic for living cells up to 100  $\mu$ g mL<sup>-1</sup>. Consequently, they are well adapted for *in vitro* imaging on cell cultures. Gd<sub>2</sub>O<sub>2</sub>S:Eu<sup>3+</sup> NPs also show strong transverse relaxivity and strong X-ray absorption allowing their use as contrast agents for  $T_2$ -weighted MRI and X-ray tomography. Our study shows that Gd<sub>2</sub>O<sub>2</sub>S:Eu<sup>3+</sup> NPs are sensibly better than commercial *Ferumoxtran-10* NPs as negative contrast agents for MRI. Upconversion emission of Gd<sub>2</sub>O<sub>2</sub>S:Er; Yb (1; 8%) NPs under infrared excitation ( $\lambda_{ex} = 980$  nm) shows mainly red emission ( $\approx$ 650–680 nm). Consequently, they are more specifically designed for *in vivo* deep fluorescence imaging, because both excitation and emission are located inside the "transparency window" of biological tissues (650–1200 nm). Magnetic relaxivity and X-ray absorption behaviors of Gd<sub>2</sub>O<sub>2</sub>S:Er; Yb NPs are almost similar to Gd<sub>2</sub>O<sub>2</sub>S:Eu<sup>3+</sup> NPs.

#### 1. Introduction

Nanoparticles (NPs) in which magnetic and optical properties coexist have been explored intensively for diverse biomedical applications, ranging from *in vivo* imaging and therapy¹ to cellular imaging and manipulation.² To date, approaches towards multimodal imaging agents have been focused on combining two different systems, such as magnetic materials and organic dyes,³ or on formulating magnetic NPs and fluorescent materials *via* polymers.⁴ Over the past decade, there have also been some recent

developments in optical bio-labeling and bio-imaging involving upconversion nanoparticles, simultaneously bringing to the forefront the desirable characteristics, strengths and weaknesses of these luminescent nanomaterials.<sup>5-7</sup>

There is an urgent need for the development of highperformance multimodal imaging agents with a simple and novel synthetic method.

We performed in our previous work, the synthesis and characterization of monodispersed  $Gd_2O_2S:Eu^{3+}$  NPs (called GADOX). This material is, in fact, a very well known scintillator which strongly absorbs X-rays and re-emits red light with a high quantum yield. Another advantage of gadolinium compounds, such as GADOX, is the high content of Gd element which is a contrast agent for MRI. Since MRI has an almost unlimited penetration depth, it allows to follow the NPs. In the same way, X-ray excitation may be used for *in vivo* tracking instead of NIR excitation used with up-converting probes.

To date, the majority of commercially available contrast agents (CAs) are  $Gd^{3+}$  chelates and many review papers on this topic have appeared in the literature over the past decades.  $^{9-11}$   $Gd^{3+}$  chelates (also called positive contrast agents) are used as  $T_1$ -weighted magnetic resonance (MR) imaging contrast agents, because they mainly shorten the longitudinal relaxation time of protons causing an increased signal intensity. More recently,

1

5

10

15

20

30

35

40

<sup>&</sup>lt;sup>a</sup>Centre d'Elaboration de Matériaux et d'Etudes Structurales, Université de Toulouse -UPS, 29 rue Jeanne Marvig, BP 94347, 31055 Toulouse, Cedex 4, France. E-mail: Robert.Mauricot@cemes.fr; Fax: +33 5 62 25 79 99; Tel: +33 5 62 25 78 49

<sup>&</sup>lt;sup>b</sup>Université Claude Bernard Lyon 1, UMR 5510, Materials: Engineering and Science, 7 avenue Jean Capelle 69622, Villeurbanne Cedex, France

<sup>&#</sup>x27;Institut Sainte Catherine, Service de radiothérapie, 1750 chemin du lavandin, Avignon, France

<sup>&</sup>lt;sup>d</sup>Biocatalysis and Organic Chemistry, Department of Biotechnology, Delft University of Technology, Julianalaan 136, 2628 BL Delft, The Netherlands

<sup>°</sup>ICELLTIS, Parc Technologique Cap delta Sud, 09340 Verniolle, France

<sup>&</sup>lt;sup>f</sup>Plateau Technique IRM, INSERM UPS/UMR 825, Pavillon Baudot, CHU Purpan, 31024 Toulouse Cedex3, France

<sup>†</sup> Electronic supplementary information (ESI) available. See DOI: 10.1039/c3nr03982i

ferumoxide, which is composed of dextran-coated superparamagnetic iron oxide (SPIO) NPs with a diameter around 150 nm, has been approved by the FDA for MRI contrast imaging on human beings, mainly for detection of liver metastases. Ferumoxide is a negative contrast agent because it causes predominant  $T_2$  (transverse relaxation time) shortening with a reduction in the signal intensity.<sup>12</sup>

In this work, we developed gadolinium oxysulfide NPs as multimodal imaging agents for  $T_2$ -weighted magnetic resonance (MR) imaging, X-ray tomography and photoluminescence (PL) imaging via hydroxycarbonate precursor precipitation followed by sulfuration under a  $H_2$ S-Ar atmosphere at 750 °C. It may be expected that these systems will gain in importance due to demand for multimodality probes and theragnostics.

## 2. Experimental section

#### 2.a. Materials

10

15

20

55

Europium, erbium, ytterbium and gadolinium nitrates (99.99%) were stock solutions from Rhodia. Urea (98%) was purchased from Sigma Aldrich.

#### 2.b. Synthesis of the precursors

Gadolinium hydroxycarbonates were synthesized as previously described.8,13 Typically, gadolinium hydroxycarbonates were synthesized from nitrate precursors in water and ethanol following a procedure based on urea decomposition at temperatures above 80  $^{\circ}$ C. The optimum concentrations used in this work were  $[Gd^{3+}] = 5.6 \times 10^{-3} \text{ M}$  and 0.5 M for urea. Europium doping concentration expressed in [Eu]/[Gd] + [Eu] (mol%) was 5. For erbium/ytterbium co-doping, the molar composition was [Er]/([Gd] + [Er] + [Yb]) = 1 and [Yb]/([Gd] + [Er])+ [Yb]) = 8. Solvent used was water-ethanol with 20 vol% of 35 ethanol. Gd, Er, Yb and Eu nitrates and urea were dissolved in the solvent, and the solution was placed in a round-bottom flask at reflux for aging at 85 °C in an oil bath, during 100 min. The suspension was then centrifuged for 30 min at 4500 rpm. The supernatant solution was discarded, and the solid phase was 40 resuspended in water and washed 3 times with water. The solid phase was then dried in an oven at 80 °C overnight.

#### 2.c. Gd<sub>2</sub>O<sub>2</sub>S NP synthesis

Gd<sub>2</sub>O<sub>2</sub>S NPs were synthesized in our laboratory and the details can be found in our earlier studies.<sup>8</sup> The sulfuration of hydroxycarbonate was carried out by solid–gas reaction as previously described.<sup>8</sup> Dried precipitates obtained were placed into a quartz tube and the sulfuration reaction was kept at 750 °C under an Ar–H<sub>2</sub>S atmosphere (83–17 vol%). After 90 min, the H<sub>2</sub>S gas flow was stopped. Only argon gas flow was supplied and samples were annealed at 850 °C for 4 h and after the samples were cooled to room temperature, Gd<sub>2</sub>O<sub>2</sub>S was obtained.

#### 2.d. Characterization techniques

Particle shape and size were examined *via* Transmission Electron Microscopy (TEM), using Philips Model CM20 and CM30 microscopes. The size was also analyzed by dynamic light

scattering (DLS) using a Zetasizer Nano (Malvern instruments). Chemical bonding was analyzed by infrared spectroscopy, using a Perkin-Elmer 100 Series spectrometer. Samples were prepared by mixing the powders with potassium bromide (1/100 by weight) in a pellet.

1

5

10

15

20

35

40

45

50

55

The luminescence of solid samples was studied with a Jobin-Yvon Model Fluorolog FL3-22 spectrometer that was equipped with a R928 Hammamatsu photomultiplier and a 450 W Xe excitation lamp. All intensities plotted on the spectra were corrected.

Water proton longitudinal relaxation times,  $T_1$ , and transverse relaxation times,  $T_2$  were measured at low field (1.4 T) with a dedicated NMR relaxometer (Bruker Minispec 60 MHz, 25 °C). The  $\rm Ln_2O_2S:Eu^{3+}$  suspensions for relaxometric studies at 1.4 T were prepared by mixing the particles with distilled water containing 1.5 wt% of agar gel as a surfactant. The  $\tau_{\rm CP}$  (half the time interval between successive 180° pulses in the CPMG pulse sequence) value was 1 ms. Relaxation rates (1/ $T_1$  and 1/ $T_2$ ) were plotted against Gd concentration values, and relaxivities ( $r_1$  and  $r_2$ ) were calculated from the slopes of the plots.

Water proton transverse relaxation times,  $T_2$ , were also measured at 7 T with a Varian-INOVA 300 NMR spectrometer and at 9.4 T with a Bruker Avance 400 NMR spectrometer. The samples were prepared by mixing the solid particles with doubly distilled water containing 1 wt% of xanthan gum as a stabilizer and for 5 min with an ultrasonic probe (Cole Parmer CV 33, 1/2'' tip, 40% amplitude, pulsed mode 10 s on/10 s off).

 $T_2$  values were measured using the Carr–Purcell–Meiboom–Gill pulse sequence (CPMG). The values of  $T_2^*$  were evaluated from the line widths. The  $T_1$  measurements were performed with the inversion recovery pulse sequence. All experimental values of relaxation rates were corrected for diamagnetic contributions using a solution of 1 wt% of xanthan in water.

Magnetic Resonance Imaging (MRI) experiments were performed using a 3 T clinical imager (Philips Achieva, located in the Unit INSERM UMRS 825, hospital Purpan, Toulouse, France). We prepared the samples of  $\rm Ln_2O_2S$  with various  $\rm Ln^{3+}$  concentrations (0–15 mM) and they were dispersed in 1.5 wt% agar–agar gel. The acquired MR image was one slice (thickness 5 mm) with a field of view of  $160 \times 120$  mm, and a voxel size of  $1 \times 1 \times 5$  mm.  $T_2$ -weighted images were acquired using a spinecho ( $T_2$ -weighted) sequence with a repetition time/echo time (TR/TE) of 1500/11 ms.

X-ray tomography scan was done at Sainte Catherine Institute, Avignon (France). Computed tomography (CT) is a GE RT16 and set from 80 to 140 kV.

#### 2.e. Cell culture, cytotoxicity test and fluorescence imaging

An indirect cytotoxicity test was performed using an elution method as described previously.<sup>14</sup> The cells used are MDA-MB231 which are triple negative breast cancer cells.<sup>15</sup> This type of cancer is one of the most aggressive. The cells were maintained in culture in RPMI 1640 medium complemented with 10% fetal bovine serum, 1% penicillin–streptomycin and incubated at 37 °C with 5% CO<sub>2</sub>. The cells were placed in 96 well plates at 10 000 cells per well. The particles were added at different concentrations to the cell medium after sonication.

Paper Nanoscale

The MTT (methylthiozoletetrazolium, Sigma) test was used to evaluate the viability of the MDA-MB231 cells in the presence of different concentrations of the NPs ( $\mathrm{Gd_2O_2S:Eu^{3^+}}$ , 5%) one and three days after their addition to cell culture medium. The MTT test is a colorimetric assay for measuring the activity of enzymes that reduce MTT to formazan dye, giving a purple color. DMSO (dimethylsulfoxide) solution is added to dissolve the insoluble purple formazan product into a colored solution. The absorbance of this colored solution can be quantified spectrophotometrically by measuring at 570 nm.

For *in vitro* labeling, cells were incubated with NPs (0.1 mg mL $^{-1}$ , 24 h) following identical conditions as for the cytotoxic test. Microscopic images were obtained using a "home made" Time Gated Luminescence Microscope (TGML) kindly built for us by Dr Dayong Jin from Macquarie University of Sydney. The main interest of a TGML is to be able to separate long lasting fluorescence coming from lanthanides from auto fluorescence coming from the biological media. $^{16}$ 

#### 3. Results and discussion

1

5

10

15

20

25

30

35

40

#### 3.a. XRD and TEM characterization of the NPs

The XRD patterns (Fig. 1) of the final products exhibit well developed peaks, characteristic of gadolinium oxysulfide; all peaks are indexed following the ICDD data in the hexagonal phase, of  $Gd_2O_2S$  (File card no. 020-1422). No extra peak coming from any impurity can be detected.

TEM images corresponding to each NP are presented in Fig. 2. NPs are spherical and mono-dispersed in size with a mean diameter of 118 nm for  $Gd_2O_2S:Eu^{3+}$  and 100 nm for  $Gd_2O_2S:Er$ ; Yb (1; 8%).

# 3.b. Photo luminescence characterization of the oxysulfide NPs

Fig. 3 shows excitation and emission spectra of  $Gd_2O_2S:Eu^{3+}$  NPs. The emission spectrum (Fig. 3a), recorded after excitation at 363 nm, exhibits the  $Eu^{3+} {}^5D_0 \rightarrow {}^7F_J (J=0-4)$  transitions. The spectrum is dominated by a strong band centered at 624 nm,

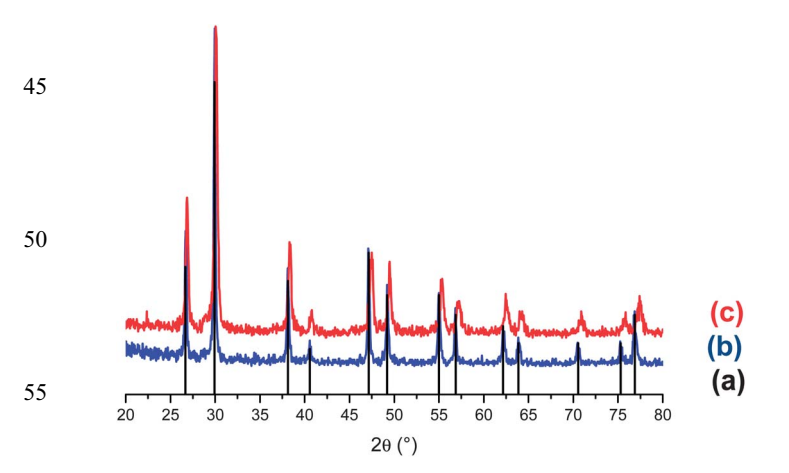


Fig. 1 XRD patterns of:  $Gd_2O_2S$  (File card no. 020-1422) (a),  $Gd_2O_2S$ : $Eu^{3+}$  (b), and  $Gd_2O_2S$ :Er; Yb (1; 8%) (c).

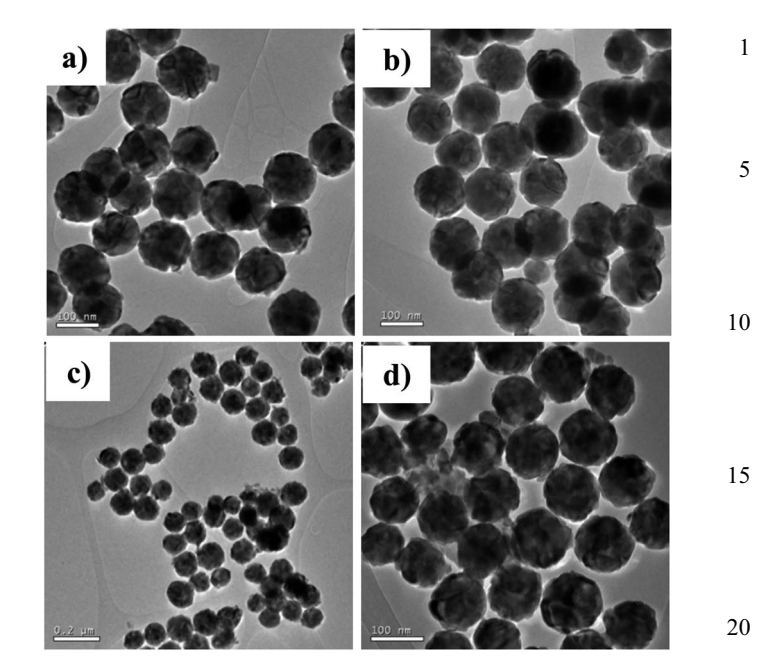
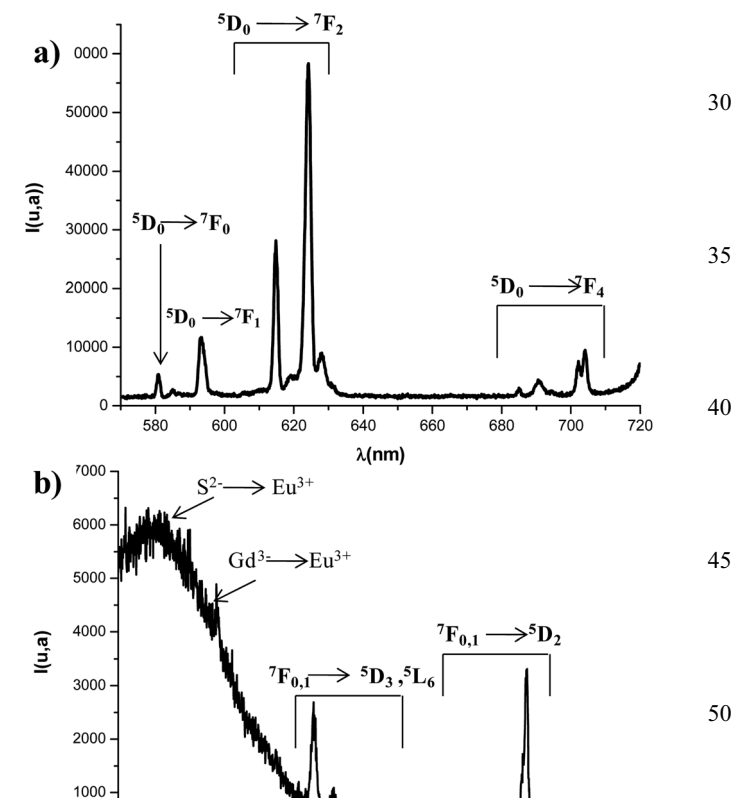


Fig. 2 TEM images of: Gd<sub>2</sub>O<sub>2</sub>S:Eu (a and b) and Gd<sub>2</sub>O<sub>2</sub>S:Er; Yb (1; 8%) (c and d).

25

55



**Fig. 3** The PL spectra of the  $Gd_2O_2S:Eu^{3+}$  sample: (a) emission spectrum under a 363 nm excitation source; (b) excitation spectrum monitored at 624 nm.

λ (nm)

characteristic of the  ${}^5D_0 \rightarrow {}^7F_2$  electric dipole transition of Eu<sup>3+</sup> ions in  $C_{3v}$  symmetry. Some  ${}^5D_1 \rightarrow {}^7F_J$  transitions are also detected. The excitation spectrum (Fig. 3b), monitored at 624 nm, can be divided into three parts, each one corresponding to an excitation mode. The narrow lines observed between 390 and 500 nm correspond to the transitions between 4f levels of Eu<sup>3+</sup>. They correspond to the direct excitation of Eu<sup>3+</sup> which is not very effective because the absorption coefficient of Eu<sup>3+</sup> is weak.

Between 390 and 320 nm, the excitation is due to the charge transfer state  $S^{2-} \rightarrow Eu^{3+}$ , centered at 355 nm. This strong absorption band is very interesting because it corresponds to the main emission band of the Hg lamp available on most commercial epifluorescence microscopes.

10

15

20

25

30

Excitation below 330 nm causes poor transmission in most optics, needs bulky, expensive and limited light sources and finally most commercial microscopes do not work in these wavelengths.

The Eu<sup>3+</sup> molar concentration for maximum red ( $^5D_0 \rightarrow {}^7F_2$ ) emission has been established in a previous study at 5 mol%.

Fig. 4 shows the upconversion emission of the  $Gd_2O_2S$ :Er; Yb (1; 8%) system under infrared excitation ( $\lambda_{ex}=980$  nm). Red emission was mainly obtained under infrared excitation, with an additional slight green emission. These peaks are assigned to the following transitions: green emission in the region of 520–560 nm assigned to the  $\{(^2H_{11/2}, ^4S_{3/2}) \rightarrow ^4I_{15/2}\}$  transition and red emission in the region of 650–680 nm assigned to the  $^4F_{9/2} \rightarrow ^4I_{15/2}$  transition for Er<sup>3+</sup> ions. The best Yb and Er concentration for maximum red (670 nm) emission has been established to Yb<sup>3+</sup> = 8 mol% and Er<sup>3+</sup> = 1 mol% after a systematic study.

It is known that the intensity of the upconversion emission I, is proportional to some power n of the excitation intensity P; *i.e.*,

35 
$$I = P^n (n = 2, 3, ...),$$
 (1)

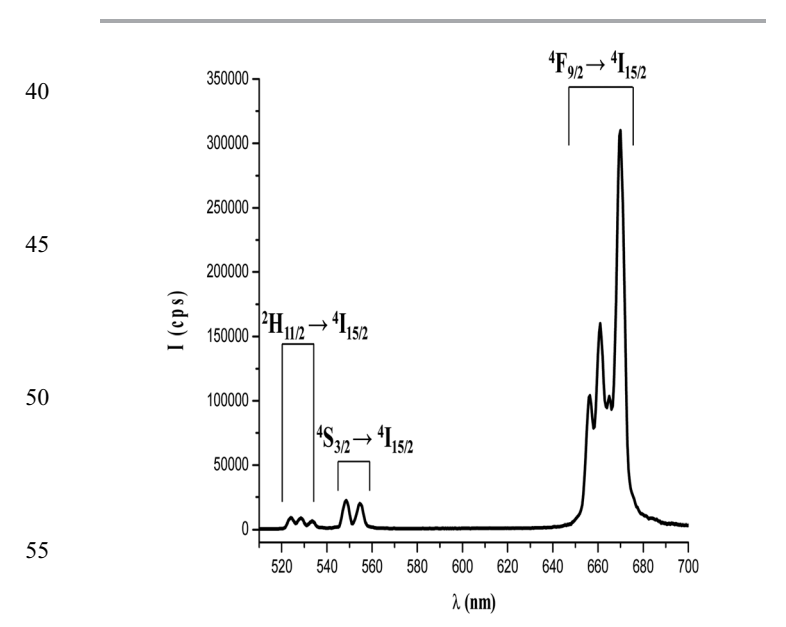


**Fig. 4** Emission spectrum of  $Gd_2O_2S:Er$ ; Yb (1; 8%) under a 980 nm excitation source with pump power.

where n is the number of pump-photons required to populate the emitting state. The number of photons of 980 nm infrared light required to excite the upconversion emissions was determined from the slope of the plot line of the laser power logarithm (log(I)) versus the upconversion emission intensity logarithm (log(P)) of the green ( ${}^4S_{3/2} \rightarrow {}^4I_{15/2}$ ) and red ( ${}^4F_{9/2} \rightarrow {}^4I_{15/2}$ ) transitions, as shown in Fig. 5. The slopes of (log(I)) versus (log(P)) are 2.38 ( $\pm$ 0.05) and 2.3 ( $\pm$ 0.06) respectively, and therefore the upconversion emission in Er<sup>3+</sup> ions occurs mainly via a two-photon process. Is,19

5

10

15

20

25

30

35

The above results on  $Gd_2O_2S:Er$ ; Yb (1; 8%) nano-phosphors should be very useful for deep (up to 1 cm) *in vivo* imaging using both excitation (980 nm) and emission (670 nm) radiation inside the "transparency window" of biological tissues (650–1200 nm).<sup>20,21</sup>

#### 3.c. Cytotoxicity tests on nanoparticles

The optical density (OD) is directly proportional to the number of cells increasing the concentration of NPs. The comparison of the proliferation of MDA-MB231 cancer cells in the presence of growing concentrations of NPs 0.1; 0.5; 1; and 2 mg mL $^{-1}$ , emphasizes a significant decrease of cell viability with high doses of NPs (>0.5 mg mL $^{-1}$ ) and shows an inhibition of cell growth whatever the time of culture (Fig. 6). However, for particle concentration around 100  $\mu g$  mL $^{-1}$  we consider that the cytotoxicity of particles is weak or negligible.

Compared to our previous work,<sup>8</sup> where we performed the same experiments on NIH3T3 mouse cells using the same Gd<sub>2</sub>O<sub>2</sub>S:Eu<sup>3+</sup>, these NPs seemed to be more cytotoxic for MDA-MB231 cancer cells showing the variability of living cells.

#### 3.d. Observation of particles fluorescence in living cells

The spherical Gd<sub>2</sub>O<sub>2</sub>S:Eu<sup>3+</sup> NPs were incubated under controlled conditions, as described in Experimental section 2.e, with MDA-

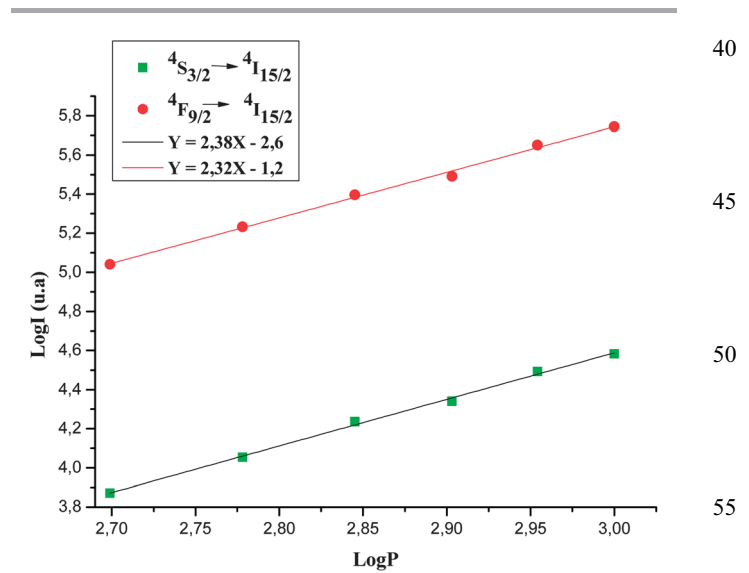


**Fig. 5** Dependence of upconversion emission intensities of Gd<sub>2</sub>O<sub>2</sub>S:Er; Yb (1; 8%) on pump power.

Paper Nanoscale

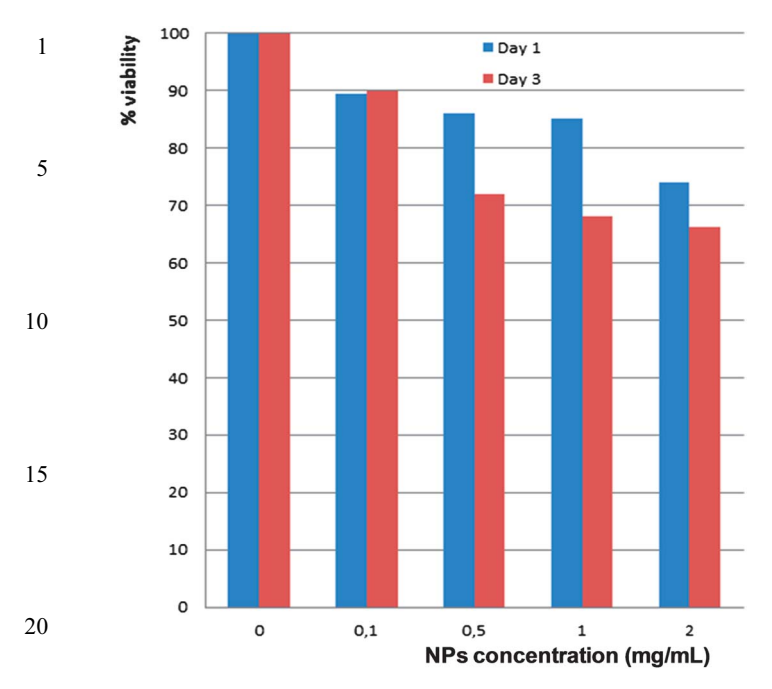


Fig. 6 Cytotoxicity test of Gd<sub>2</sub>O<sub>2</sub>S:Eu<sup>3+</sup> NPs.

25

30

40

45

50

55

MB231 cancer cells. The results show (Fig. 7) that NPs have been internalized by the cells. Indeed, a strong red fluorescence is observed in their cytoplasm with a higher intensity in the perinuclear area. The nucleus, stained in blue with DAPI, appears to be totally free of NPs as shown by time gated detection.

# 3.e. Longitudinal and transverse relaxivity measurements; MR imaging of the oxysulfide NPs

The efficacy of the NPs as  $T_1$ - or  $T_2$ -weighted MR contrast agents was evaluated by measuring the longitudinal  $(r_1)$  and the transverse  $(r_2)$  nuclear magnetic relaxation rates of water protons in aqueous suspensions at low and high field.

**Low field study (1.4 T).** The longitudinal  $(T_1)$  and transverse  $(T_2)$  relaxation times were measured at different  $Gd^{3+}$  ion

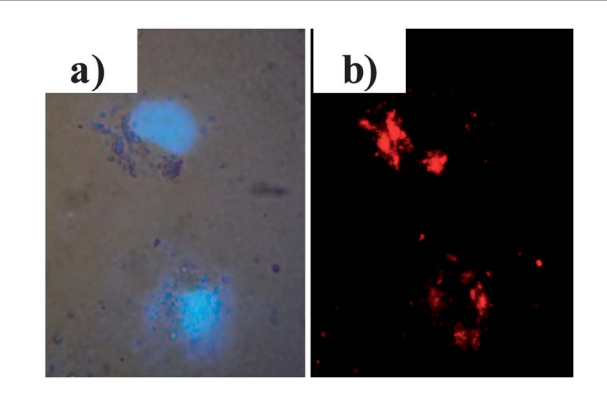


**Fig. 7** Internalization of  $Gd_2O_2S:Eu^{3+}$  NPs in MDA-MB231 cancer cells after exposure to  $Gd_2O_2S:Eu^{3+}$  NPs (overnight, 0.1 mg mL $^{-1}$ ). (a) Representative bright field images + UV excitation ( $\lambda_{ex}$ : 365 nm, the blue color comes from the nucleus colored with DAPI used to help cell detection). (b) UV excitation ( $\lambda_{ex}$ : 365 nm) and time gated detection of  $Gd_2O_2S:Eu^{3+}$  NPs.

concentrations. The  $r_1$  and  $r_2$  values were then determined from the plot slopes of  $1/T_1$  (= $R_1$ ) and  $1/T_2$  (= $R_2$ ) *versus* the Gd<sup>3+</sup> ion concentration and the results are presented in Table 1.

1

5

10

15

20

30

35

40

45

50

55

MR contrast agents can be classified according to their  $T_1$  or  $T_2$  enhancement capability. When the  $r_2/r_1$  value is close to 1.0, application as a positive contrast agent is favored. On the other hand, when this ratio is larger, the contrast agents are viewed as negative contrast agents.<sup>22</sup>

The longitudinal relaxivities  $r_1$  (see Table 1) were very small for  $\mathrm{Gd_2O_2S:Eu^{3^+}}$  NPs compared to  $\mathrm{Gd\text{-}DOTA}$  – gadoterate meglumine ( $r_1=3.4\,\mathrm{s^{-1}}\,\mathrm{mM^{-1}}$  and  $r_2=4.8\,\mathrm{s^{-1}}\,\mathrm{mM^{-1}}$  at 1 Tesla; 37 °C),<sup>23</sup> which suggests that the amount of water in close contact with the  $\mathrm{Ln^{3^+}}$  ion is limited, probably because of the relatively big size of these particles. Surely, these NPs will not show good performance as positive contrast agents. However, the quite good  $r_2$  value at low field is more promising. The ratio  $r_2/r_1$  increased from 33 to 66 along with the NPs radius increase from 25.5 nm to 110 nm (see also Table 1). It indicates that  $\mathrm{Gd_2O_2S:Eu^{3^+}}$  NPs are more likely to be used as negative MR contrast agents (short  $T_2$  relaxation time).

High field study (7 and 9.4 T). The transverse relaxation rates determined using the Carr–Purcell–Meiboom–Gill ( $R_2$ ) pulse sequence appeared to be strongly dependent on  $\tau_{\rm CP}$  (half the time interval between two refocusing pulses). The relaxivities of  $Gd_2O_2S:Eu^{3+}$  are compiled in Table 2.

The observed trends appeared to be similar to those reported previously for  $\rm Ln_2O_3$  NPs and this behavior is typical for the static dephasing regime (SDR),<sup>24</sup> where the condition  $\tau_{\rm D} < \Delta \omega (r_{\rm p})^{-1}$  holds ( $\tau_{\rm D} = r_{\rm p}^2/D$ ), where  $r_{\rm p}$  is the radius of the particle, D is the water diffusion coefficient and  $\Delta \omega (r_{\rm p})$  is the difference in Larmor frequency of the water protons located at the surface of the particle and those at infinity. By contrast, dextran coated  $\rm Dy_2O_3$  NPs<sup>25</sup> and  $\rm Ho_2O_3$  NPs stabilized by addition of 0.05% (w/w) of the cationic surfactant cetyltrimethylammonium bromide (CTAB)<sup>26</sup> to the dispersion showed a behavior that is typical for the outer sphere regime (OS) with nearly equal values of  $R_2$  and  $R_2$ \* (in both cases no xanthan was needed to prevent precipitation). Therefore, the SDR behavior of the presently studied systems and of the previously studied  $\rm Ln_2O_3$  NPs can be ascribed to the adsorption of a thick layer of xanthan on the NPs.

The transverse relaxivities ( $r_2$  and  $r_2$ \*) were fitted to a model that has successfully been applied previously for the rationalization of the transverse relaxivities of  $Ln_2O_3$  NPs.<sup>25</sup> Under SDR conditions,  $R_2$ \* can be ascribed to the dephasing of motionless magnetic moments in a non-uniform magnetic field created by the randomly distributed NPs. The value of  $R_2$ \* is then given by eqn (2), where f is the volume fraction occupied by the NPs and  $R_2^0$  is the contribution due to other relaxation mechanisms such

**Table 1** Relaxivities  $r_i$  (s<sup>-1</sup> mM<sup>-1</sup>, i = 1, 2) of aqueous suspensions containing agar gel (1.5 wt%) of Gd<sub>2</sub>O<sub>2</sub>S:Eu<sup>3+</sup> at B = 1.4 T and T = 25 °C

$r_{\text{TEM}} (\text{nm})$	$r_2 \left( s^{-1} \text{ mM}^{-1} \right)$	$r_1 \left( s^{-1} \text{ mM}^{-1} \right)$	$r_2/r_1$
25.5	15	0.46	32.6
59	20.1	0.33	60.9
110	24.9	0.38	65.6

**Table 2** Relaxivities of aqueous suspensions of gadolinium oxysulfide at B=7 T and T=25 °C<sup>a</sup>

Material	$\frac{r_{\rm p}}{({\rm nm})^b}$	$\binom{r_1}{(s^{-1} \text{ mM}^{-1})}$	$(s^{-1} \text{ mM}^{-1})^c$	$r_2^*$ (s <sup>-1</sup> mM <sup>-1</sup> )	$\Delta\omega(r_{ m p}) \ (10^6~{ m s}^{-1})^d$	$\frac{\Delta\omega(r_{\rm p})_{\rm max}}{(10^6~{\rm s}^{-1})^e}$	$\begin{array}{c} \tau_{\rm D}(r_{\rm diff}) \\ \left(10^{-4} \; {\rm s}\right)^d \end{array}$	$r_{ m p}/r_{ m diff}{}^d$	$r_{\rm p} ({\rm nm})^f$	$r_{\rm diff} ({\rm nm})^f$
Gd <sub>2</sub> O <sub>2</sub> S:Eu <sup>3+</sup>	25.5	0.24	55	483	$7.763 \pm 0.025$	7.772	$38 \pm 49$	$0.022 \pm 0.009$	59.9	2673.4
Gd <sub>2</sub> O <sub>2</sub> S:Eu <sup>3+</sup>	30.0	0.24	48	490	$7.872 \pm 0.005$	7.772	$211\pm24$	$0.0114 \pm 0.0004$	72.2	6330.2
Gd <sub>2</sub> O <sub>2</sub> S:Eu <sup>3+</sup>	59.0	0.23	114	639	$10.263 \pm 0.011$	7.772	$401\pm33$	$0.0106 \pm 0.0003$	92.3	8731.3

 $^a$  1 wt% xanthan.  $^b$  From TEM.  $^c$  At  $au_{\rm CP}=5$  ms.  $^d$  From fitting of experimental data with eqn (2) and (3).  $^e$  Calculated with magnetization of a single particle.  $^f$  Calculated from the best-fit values of  $au_{\rm CP}(r_{
m diff})$ ,  $r_{
m p}/r_{
m diff}$ ,  $D_0=1.9\times10^{-9}~{
m m}^2~{
m s}^{-1}$ , and  $R_2^0=0$ .

as exchange. For the calculation of  $R_2$ , a imaginary sphere around the particle is defined with radius  $r_{\rm diff}$  for which  $\tau_{\rm D}(r_{\rm diff}) = 1/\Delta\omega(r_{\rm diff})$  and which forms the border between contributing and non-contributing proton spins to  $R_2$  (e.g., of very slowly diffusing water molecules in the xanthan layer). Application of the theory of weak magnetic particles leads to eqn (3).<sup>27</sup> The fitting was performed using  $\Delta\omega(r_{\rm p})$ ,  $\tau_{\rm D}(r_{\rm diff})$ , and  $r_{\rm p}/r_{\rm diff}$  as adjustable parameters.

5

10

15

20

30

35

40

50

55

$$R_2^* = \frac{1}{T_2^*} = R_2^0 + \frac{2\pi\sqrt{3}f\Delta\omega(r_p)}{9}$$
 (2)

$$R_{2} = R_{2}^{*} + \frac{\left[\Delta\omega\left(r_{\text{diff}}\right)\right]^{2} f\left(r_{\text{diff}}\right) \tau_{D}\left(r_{\text{diff}}\right) F(x)}{2}$$

$$\text{where } F(x) = \frac{1}{\sqrt{\pi}} \int_{0}^{\infty} dy \frac{e^{-y}}{\sqrt{y}} \left[1 - \frac{1}{xy} \tanh(xy)\right] \text{ and } x = \frac{4\tau_{\text{CP}}}{\tau_{D}(r_{\text{diff}})}.$$

The values of  $\Delta\omega(r_{\rm diff})$ ,  $\tau_{\rm D}(r_{\rm diff})$  and  $f(r_{\rm diff})$  can be expressed as follows:

$$\Delta\omega(r_{\rm diff}) = \Delta\omega(r_{\rm p}) \left(\frac{r_{\rm p}}{r_{\rm diff}}\right)^3 \tag{4}$$

$$\tau_{\rm D}(r_{\rm diff}) = \tau_{\rm D}(r_{\rm p}) \left(\frac{r_{\rm diff}}{r_{\rm p}}\right)^2 \left(\frac{D}{D_0}\right) \tag{5}$$

$$f(r_{\text{diff}}) = f(r_{\text{p}}) \left(\frac{r_{\text{diff}}}{r_{\text{p}}}\right)^{3} \tag{6}$$

When  $R_2^0$  was adjustable, negative values for some of the other adjustable parameters or best-fit results with very large standard deviations were obtained. Therefore,  $R_2^0$  was fixed at 0. Very good agreement between the experimental and calculated values was achieved. The best-fit parameters are listed in Table 2. From the values of  $\tau_D(r_{\text{diff}})$  and  $D_0 = 1.9 \times 10^{-9} \text{ m}^2 \text{ s}^{-1}$ , the values for  $r_{\rm diff}$  were calculated. From the latter and the best-fit parameters,  $r_p$  was calculated. The values obtained were in reasonably good agreement with the values obtained from TEM, considering the crudeness of the model. Since,  $r_{\rm diff}$  is the radius of the sphere, within which water protons are silent with regard to transverse relaxivity; it also reflects the thickness of the xanthan layer around the particle. From the obtained values it can be estimated to be 3–10  $\mu$ m, which is an order of magnitude thicker than for the previously studied Ln<sub>2</sub>O<sub>3</sub> nanoparticles.<sup>25</sup> Another difference with the previously studied particles is that the best-fit values for  $\Delta\omega(r_{\rm p})$  for the smallest NPs (25–35 nm) are in good agreement with the maximum calculated values for this

parameter. In the previous study on  $\rm Ln_2O_3$  NPs, the evaluated values for  $\Delta\omega(r_{\rm p})$  were significantly smaller than the calculated values for  $\Delta\omega(r_{\rm p})_{\rm max}$ , which may be explained by the difference in their shapes. The previously studied material consisted, in the solid state, of fiber-like aggregates of plates with a size of 5–10 nm. In suspension, these aggregates disrupted into smaller aggregates with a radius of 50–100 nm. A non-spherical shape of those particles may explain the relatively low values for  $\Delta\omega(r_{\rm p})$ . In the previous study, in contrast to the present one, large values for  $R_2^0$  were needed to obtain good fits. Probably,  $R_2^0$  is mainly determined by exchange of water protons between the bulk and, for instance, intra-aggregate water protons which have a large chemical shift difference due to the neighboring paramagnetic  ${\rm Ln}^{3^+}$  ions.  $^{28}$ 

5

10

15

20

30

35

40

45

50

55

It should be noted that the evaluated values of  $\Delta\omega(r_{\rm p})$  for the larger  ${\rm Gd_2O_2S}$  particles (59–85 nm) are significantly higher than the calculated maximum values. Possibly magnetic interactions between the  ${\rm Gd}^{3+}$  ions and the  ${\rm Eu}^{3+}$  ions lead to  $\mu_{\rm eff}$  higher values and thus to higher relaxivities.

The relaxivities of the  $Gd_2O_2S$  NPs clearly demonstrate the effect of the radius. From the evaluated parameters, it can be concluded that the increase of the transverse relaxivities along with the particle size increase can be rationalized by the increase of  $\tau_D(r_{\rm diff})$ .

The transverse relaxivities are proportional to the effective magnetic moment of the system under study.

At B=7.1 T, the relaxivities of the  ${\rm Gd_2O_2S}$  NPs studied are in general better than those of commercial iron oxide based negative contrast agents. For example, the  $r_2$  value of  ${\rm Gd_2O_2S}$  NPs of 59 nm in radius, is higher than that of *Ferumoxtran-10* (AMI-227) which has  $r_2=71$  s<sup>-1</sup> mM<sup>-1</sup> at B=7.1 T.<sup>29</sup>

The suspensions of the  $Gd_2O_2S$  NPs were also studied at a magnetic field strength of 9.4 T. The results show that both  $r_2$  and  $r_2$ \* are linearly proportional to the magnetic field strength *B*. Fig. 8 shows the case of  $Gd_2O_2S:Eu^{3+}$ .

The value of  $r_2$  varies linearly with the field whatever the particle size. This linear dependence confirms that the SDR holds for these NPs under the conditions applied; for the OS mechanism a quadratic dependence of B would be expected.<sup>30</sup>

The longitudinal relaxivities of the  $Gd_2O_2S$  systems at 7.1 (see Table 2) are lower than those at 1.4 T, which is in agreement with the general trend predicted by the Solomon–Bloembergen–Morgan equations for slowly tumbling systems above about 1.5 T.<sup>10</sup>

At present, there is a tendency to perform MRI examinations at higher magnetic fields. Gadolinium oxysulfide has favorable  $T_2$ -weighted relaxivity properties for high field MRI. It should be

Paper Nanoscale

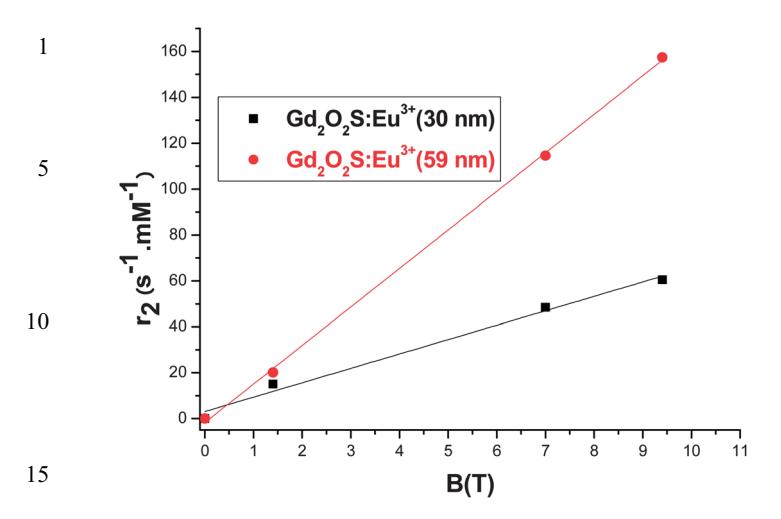


**Fig. 8** Dependence of the transverse relaxivity of aqueous suspension of  $Gd_2O_2S$ : $Eu^{3+}$  on the external magnetic field B.

noted however, that various factors are important for application in molecular imaging, including the toxicity protection of the particle by the coating for leaching, and the effect of the particle size on the biodistribution. Further research to confirm this is required.

20

25

MR imaging. We evaluated whether Gd<sub>2</sub>O<sub>2</sub>S:Eu<sup>3+</sup> and Gd<sub>2</sub>O<sub>2</sub>S:Er; Yb (1; 8%) NPs were usable as negative CAs in magnetic resonance imaging (MRI). We performed *in vitro* MR

assays ( $T_2$ -weighted imaging) in 1.5 wt% agar gel for both types of NPs using a series of Gd<sup>3+</sup> concentrations (range 0–15 mM).  $T_2$ -weighted imaging, both NPs made the images darker at higher Gd<sup>3+</sup> concentrations (Fig. 9), and the signal intensity decreased. This is confirmed by the intensity profile measurement.

1

5

10

15

20

25

This attenuation of the signal intensity is much larger when the NP radius increases. Thus the transverse relaxation time  $T_2$  becomes shorter when the NP size increases. These results confirm those obtained during the relaxometric studies and proved the usability of  $\mathrm{Gd_2O_2S:Eu^{3+}}$  and  $\mathrm{Gd_2O_2S:Er}$ ; Yb (1; 8%) NPs as negative CAs in magnetic resonance imaging.

#### 3.f. X-ray computed tomography

To investigate the *in vitro* Computed Tomography (CT) imaging of  $Gd_2O_2S:Eu^{3+}$  NPs, 7 phantom samples, containing an increasing amount of NPs, were embedded in a perforated plastic plate (Fig. 10).

The darkest spot represents the empty hole, which had no absorption. Sample 0 containing agar gel (1.5% wt), was used as a control. The X-rays were absorbed efficiently by the samples, and the intensity of the CT value increased as the concentration of the samples increased. Then, X-ray absorption increases with Gd concentration and thus with the electron density of the sample. From a concentration around 4 mM of Gd we can clearly detect the sample spot on the CT image. Thus, the

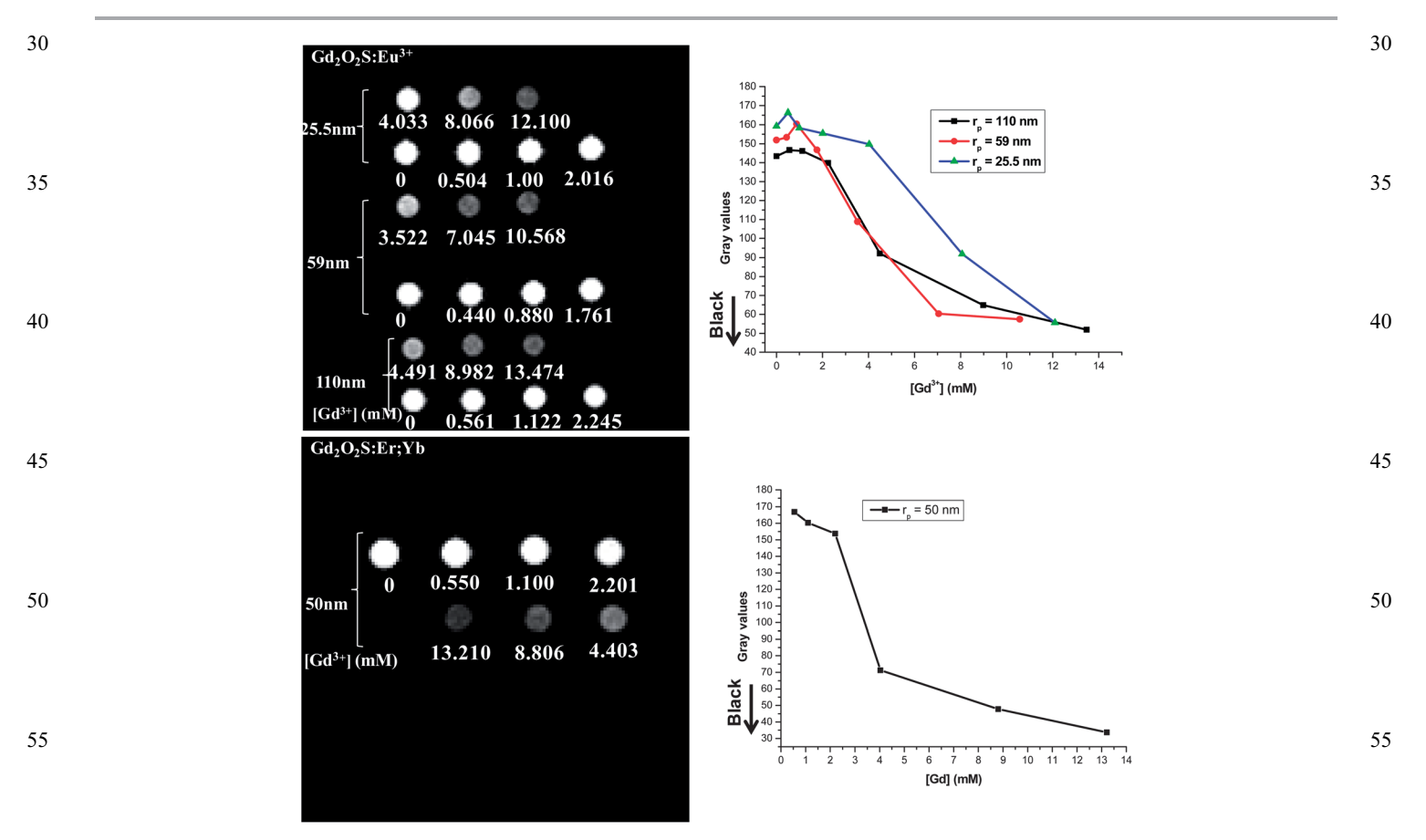


Fig. 9 T<sub>2</sub>-weighted MR imaging of Gd<sub>2</sub>O<sub>2</sub>S:Eu<sup>3+</sup> and Gd<sub>2</sub>O<sub>2</sub>S:Er; Yb (1; 8%) NPs with intensity profile measurements.

1

10

15

20

25

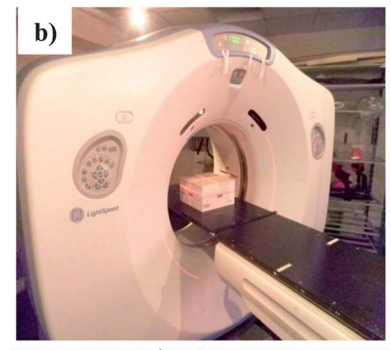
30

35

40

50

55



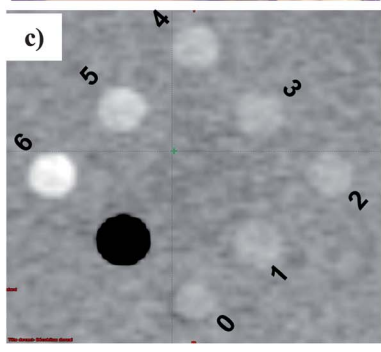


**Fig. 10** (a) Plate image "phantom" filled with holes containing  $Gd_2O_2S:Eu^{3+}$  NPs suspended in an agar gel, (b) plate image inside the CT, and (c) CT image (100 kV): 0: control, 1: 0.52 mM, 2: 1.04 mM, 3: 2.08 mM, 4: 4.15 mM, 5: 8.3 mM, and 6: 16.6 mM

Gd<sub>2</sub>O<sub>2</sub>S:Eu<sup>3+</sup> NPs could be potentially applied as a CT imaging contrast agent.

When the sample is irradiated with X-rays, it produces radiation–matter interactions such as absorption and Compton scattering. The effect of X-ray attenuation on CT image was studied by measuring the mean Hounsfield Unit (HU) variation of the acquired image depending on Gd concentration at different voltages of used energy. Phantom images were treated using a standard image viewer application (scanner). Fig. 11 shows a linear relationship between NP concentration and the shift in HU from the background.

This figure also shows that the contrast effect is more effective for low energy (80 kV) than for higher energy (140 kV). Note that  $Gd_2O_2S:Eu^{3+}$  NP behavior is exactly opposite to gold NPs which give a better contrast effect at high energy (140 kV) than at lower (80 kV).<sup>31</sup> This difference is clearly observed for  $[Gd^{3+}] \approx 16.6$  mM. When  $[Gd^{3+}] < 4$  mM the number of Hounsfield units is less than 30 which we can assume is the limit to visualize the target against a background.

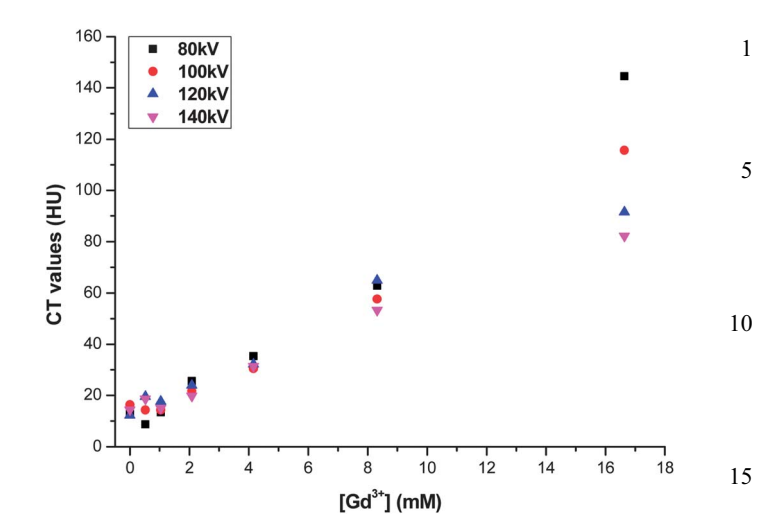


Fig. 11 Plot of ΔHU *versus* Gd<sub>2</sub>O<sub>2</sub>S:Eu<sup>3+</sup> concentration in agar–agar phantom.

20

30

35

40

45

55

# 4. Conclusion, additional comments and perspectives

We have synthesized gadolinium oxysulfide NPs as multimodal imaging agents for  $T_2$ -weighted MR imaging, X-ray tomography and photoluminescence imaging.  $Gd_2O_2S:Eu^{3+}$  NPs strongly absorb X-rays or near UV (363 nm) and re-emit red light with a high intensity. They are well adapted for *in vitro* fluorescence microscopy, MR imaging and X-ray tomography.

Upconversion emission of the  $Gd_2O_2S:Er$ ; Yb system under infrared excitation ( $\lambda_{ex}=980$  nm) showed mainly red emission centered around 670 nm. Consequently, these NPs are more specially designed for deep *in vivo* fluorescence imaging, because both excitation and emission are located inside the "transparency window" of biological tissues (650–1200 nm).

The  $r_2$  value (114 s<sup>-1</sup> mM<sup>-1</sup> at B=7 T) of Gd<sub>2</sub>O<sub>2</sub>S NPs for a radius of 59 nm, is higher than for *Ferumoxtran-10* (*Sinerem*) ( $r_2=71~{\rm s^{-1}}$  mM<sup>-1</sup> at B=1.5 T), almost equal to Endorem ( $r_2=120~{\rm s^{-1}}$  mM<sup>-1</sup> at B=1.5 T) and slightly lower than for Resovist ( $r_2=r_{\rm diff}$  190 s<sup>-1</sup> mM<sup>-1</sup> at B=1.5 T) which are very well known commercial iron oxide negative contrast agents. However comparison must be done with care because the  $T_2$  relaxivity of gadolinium oxysulfide NPs increases with the magnetic field whereas the transverse relaxivity of iron oxide particles increases with the magnetic field for low fields. Only at stronger fields, it will decrease. The particle size has also an influence here. Consequently, gadolinium oxysulfide NPs will be mainly interesting for high field and high resolution MRI (>3 T) where other contrast agents saturate.

X-rays are efficiently absorbed by  $Gd_2O_2S:Eu^{3^+}$  NPs, and the contrast detected by Computed Tomography (CT) increased linearly as the concentration of the samples increased. Clear contrast can be detected on CT images beyond a concentration of 4 mM of Gd. Consequently, this work has clearly demonstrated the high potentiality of gadolinium oxysulfide NPs doped with other lanthanides ( $Eu^{3^+}$ ,  $Er^{3^+}$ ,  $Yb^{3^+}$ ) as multimodal imaging agents.

**Paper** Nanoscale

These Gd<sub>2</sub>O<sub>2</sub>S NPs have been characterized without any functionalization because any surface change will modify both the luminescence and relaxivity properties. Consequently, data reported here constitute the reference before any surface modification for biological application. These nude Gd<sub>2</sub>O<sub>2</sub>S NPs are hydrophiles and a colloidal suspension in pure water is quite stable. Suspension in agar gel, leads to well dispersed unmoving particles allowing precise relaxivity measurements. However, the ionic strength of physiological serum causes an 10 **5** immediate flocculation avoiding any biological use without surface modification.

1

15

20

30

35

Suspension of Gd<sub>2</sub>O<sub>2</sub>S NPs in water or physiological serum does not degrade the nano-objects even after several weeks and no release of toxic Gd<sup>3+</sup> is detected. Moreover, as preliminary trials we have injected (in the tail vein) to five mice (C57 black mouse), 200 μL of a 3.3 mg mL<sup>-1</sup> of Gd<sub>2</sub>O<sub>2</sub>S NPs dispersed in physiological serum using polyethylene glycol (mol wt 3000) as a dispersing agent with  $[Gd^{3+}]/[PEG] = 5$ . Dynamic Light Scattering (DLS) measurements and photographs of the colloidal suspension were obtained and presented in the ESI.† As expected, Gd<sub>2</sub>O<sub>2</sub>S NPs move quickly (5 minutes) into the liver and kidneys where they give a strong negative contrast easily detected by MRI. The contrast is maximum after 50 minutes and remains almost constant for 15 days. After one month, the contrast begins to decrease little by little and disappears totally after 4 months showing that even if Gd<sub>2</sub>O<sub>2</sub>S NPs are very stable, they are finally eliminated by the body. During this preliminary trial, no mouse died and no mouse showed any pathology, weight loss or abnormal behavior. This preliminary toxicity test will be soon completed by further studies and will be the topic of the next publication.

# Abbreviations and acronyms

	NPs	nanoparticles
	CA	contrast agent
	MR	magnetic resonance
40	MRI	magnetic resonance imaging
	NMR	nuclear magnetic resonance
	OS	outer sphere
	SDR	static dephasing regime
	D	relative diffusion constant
45	$r_{ m diff}$	radius of a sphere around a particle inside which
		refocusing pulses are fully effective
	$R_i = 1/T_i$	relaxation rate $(i = 1, 2)$
	$r_i$	relaxation rates expressed in s <sup>-1</sup> mM <sup>-1</sup>
		concentration of paramagnetic ions $(i = 1, 2)$
50	$r_{ m p}$	radius of a particle
	$T_1$	longitudinal proton relaxation time
	$T_2$	transverse proton relaxation time
	$T_2$ *	observed time constant of the free induction
		NMR signal
55	$ au_{ ext{CP}}$	half the time interval between successive 180°
		pulses in the CPMG pulse sequence
	$ au_{\mathbf{D}}$	diffusion correlation time, $\tau_{\rm D} = r^2/D$ ( $r$ , particle
		radius; D, diffusion coefficient)
	CT	Computed Tomography.

## **Acknowledgements**

The "Agence National de la Recherche" (ANR) and the "Pôle de Compétitivité Cancer Bio Santé" from the Midi-Pyrénées region are thanked for their support of the PDTX program.

1

5

10

15

20

25

30

35

40

45

50

55

#### References

- 1 J. Kim, Y. Piao and T. Hyeon, Chem. Soc. Rev., 2009, 38, 372-
- 2 J. H. Lee, E. S. Kim, M. H. Cho, M. Son, S. I. Yeon, J. S. Shin and J. Cheon, Angew. Chem., Int Ed., 2010, 49, 5698-5702.
- 3 J. E. Lee, N. Lee, H. Kim, J. Kim, S. H. Choi, J. H. Kim, T. Kim, I. C. Song, S. P. Park, W. K. Moon and T. Hyeon, J. Am. Chem. Soc., 2010, 132, 552-557.
- 4 K. J. Chen, S. M. Wolahan, H. Wang, C. H. Hsu, H. W. Chang and A. Durazo, Biomaterials, 2011, 32, 2160-2165.
- 5 F. Wang, D. Banerjee, Y. Liu, X. Chen and X. Liu, Analyst, 2010, 135, 1839-1854.
- 6 F. Wang, Y. Han, C. S. Lim, Y. Lu, J. Wang, J. Xu, H. Chen, C. Zhang, M. Hong and X. Liu, *Nature*, 2010, 463, 1061-1065.
- 7 W. Fan, B. Shen, W. Bu, F. Chen, K. Zhao, S. Zhang, L. Zhou, W. Peng, Q. Xiao, H. Xing, J. Liu, D. Ni, Q. He and J. Shi, J. Am. Chem. Soc., 2013, 135, 6494-6503.
- 8 S. A. Osseni, S. Lechevallier, M. Verelst, C. Dujardin, J. Dexpert-Ghys, D. Neumeyer, M. Leclercq, H. Baaziz, D. Cussac, V. Santran and R. Mauricot, J. Mater. Chem., 2011, 21, 18365.
- 9 J. A. Peters, J. Huskens and D. J. Raber, Prog. Nucl. Magn. Reson. Spectrosc., 1996, 28, 283-350.
- 10 P. Caravan, J. J. Ellison, T. J. McMurry and R. B. Lauffer, Chem. Rev., 1999, 99, 2293-2352.
- 11 C. F. G. C. Geraldes and S. Laurent, Contrast Media Mol. Imaging, 2009, 4, 1-23.
- 12 E. Senéterre, P. Taourel, Y. Bouvier, J. Pradel, B. Van Beers, J. P. Daures, J. Pringot, D. Mathieu and Bruel, Radiology, 1996, 3, 785-792.
- 13 S. Lechevallier, P. Lecante, R. Mauricot, H. Dexpert, J. Dexpert-Ghys, H. Kong, H. K. Kong, G. L. Law and K. L. Wong, Chem. Mater., 2010, 22, 6153-6161.
- 14 T. Mosmann, J. Immunol. Methods, 1983, 65, 55-63.
- 15 B. R. Brinkley, P. T. Beall, L. J. Wible, M. L. Mace, S. T. Donna and R. M. Cailleau, Cancer Res., 1980, 40, 3118-3129.
- 16 J. Dayong and P. A. James, Anal. Chem., 2011, 83(6), 2294-2300.
- 17 F. E. Auzel, Proc. IEEE, 1973, 61, 758-786.
- 18 M. Pollnau, D. R. Gamelin, S. R. Lüthi and H. U. Güdel, Phys. Rev. B: Condens. Matter Mater. Phys., 3337.
- 19 H. R. Page, K. I. Schaffers, P. A. Waide, J. B. Tassano, S. A. Payne and W. F. K. Krupke, J. Appl. Phys., 1972, 43, 595-600.
- 20 Y. Yang, Q. Shao, R. Deng, C. Wang, X. Teng, K. Cheng, Z. Cheng, L. Huang, Z. Liu, X. Liu and B. Xing, Angew. Chem., Int. Ed., 2012, 51, 3125-3129.
- 21 M. Haase and H. Schäfer, Angew. Chem., Int. Ed., 2011, 50, 5808-5829.

- 22 M. A. Fortin, R. M. Petoral, J. F. Soderlind, A. Klasson, M. Engstrom, T. Veres, P. O. Kall and K. Uvdal, *Nanotechnology*, 2007, **18**, 395501.
  - 23 S. Laurent, D. Forge, M. Port, A. Roch, C. Robic, E. L. Vander and R. N. Muller, *Chem. Rev.*, 2008, **108**, 2064–2110.
  - 24 M. Norek, G. A. Pereira, C. F. G. C. Geraldes, A. Denkova, W. Zhou and J. A. Peters, *J. Phys. Chem. C*, 2007, **111**, 10240–10246.
  - 25 M. Norek, E. Kampert, U. Zeitler and J. A. Peters, *J. Am. Chem. Soc.*, 2008, **130**, 5335–5340.
- 10 26 F. Mayer, J. A. Peters and K. Djanashvili, *Chem.–Eur. J.*, 2012, **18**, 8004–8007.

- 27 J. H. Jensen and R. Chandra, *Magn. Reson. Med.*, 2000, 44, 144–156.
- 28 Q. L. Vuong, P. Gillis and Y. Gossuin, *J. Magn. Reson.*, 2011, 212, 139–148.
- 29 M. M. J. Modo, J. W. M. Bulte and E. E. Kim, *J. Nucl. Med.*, 2007, 48, 2087.
- 30 M. Norek and J. A. Peters, *Prog. Nucl. Magn. Reson. Spectrosc.*, 2011, **59**, 64–82.
- 31 E. Boote, G. Fent, V. Kattumur, S. Casteel, K. Katti, N. Chanda, R. Kannan, K. Katti and R. Churchill, *Acad. Radiol.*, 2010, 17, 410–417.